Journal of Physics:
Conference Series

Two-point enstrophy budget and energy cascade in turbulence

Journal of Physics: Conference Series **3173** (2026) 012029 doi:10.1088/1742-6596/3173/1/012029

Two-point enstrophy budget and energy cascade in turbulence

A. Cimarelli[1], C.B. da Silva[2] and G. Boga[1]

[1]DIEF, University of Modena and Reggio Emilia, 41125 Modena, Italy
[2]IDMEC/IST, Technical University of Lisbon, 1049-001 Lisboa, Portugal

E-mail: andrea.cimarelli@unimore.it

Abstract. According to the Kolmogorov's four-fifths law, the prominent feature of high Reynolds number flows is the energy transfer from large to small scales which is described by a single scalar quantity, the average dissipation rate. Kolmogorov's groundbreaking intuition was reducing the complex problem of turbulence to its essential features, by assuming homogeneity and isotropy. However, actual turbulent flows have a much richer physics, involving, beyond energy transfer, anisotropic production and inhomogeneous spatial fluxes. The energy injection/release associated with these phenomena gives rise to a split cascade where energy flows simultaneously both to small and large scales. The split in forward and reverse cascade is particularly relevant in wall turbulence where it challenges turbulence closures and theories. To shed light on these processes, we consider the exact evolution equations for the second-order moment of the two-point velocity and vorticity increments. Preliminary results on the flow settings of a temporally evolving boundary layer are presented and are shown to unveil interesting physical mechanisms at the basis of the split cascade phenomenon.

1 Introduction

Since the seminal work of Kolmogorov (1941), no revolutionary steps have been made in the development of a universal theory of turbulence. Many of the theoretical results concern isotropic homogeneous turbulence, while a unique theory capable of explaining most of the phenomena occurring in every day flows is completely missing. Considerable effort has been certainly spent in investigating the canonical flows, which consist in relatively simple flow configurations that allow to grasp some essential features and concepts that are also applicable to more general cases. Among this family of flow configurations, it is possible to identify a group of cases of interest for the study of wall turbulence: the channel flow, the pipe flow and the boundary layer. Among these three configurations the only one presenting a turbulent/non-turbulent interface, across which the turbulent entrainment phenomenon occurs, is the boundary layer [1].

The presence of a solid boundary strongly modifies the classical picture of turbulence. The strong inhomogeneity and anisotropy imposed by the presence of a wall and of a mean shear challenges the development of a complete theory able to explain and predict the interplay between the elementary phenomena governing the flow. In the family of wall turbulent flows it is common to identify different regions based on their features. In the near-wall region, the production of turbulent fluctuations exceeds their dissipation rate. The excess is transported towards the wall and towards the bulk region, where is finally dissipated. The near-wall layer is certainly crucial to the dynamics of attached shear flows: it is dominated by intense interacting structures [2, 3] and is the seat of the highest rate of turbulent energy production and of the highest turbulent intensities. In this region, turbulence is sustained by a

self-sustaining and autonomous cycle [4]. The strong anisotropy and inhomogeneity of this region strongly affects the energy cascade mechanism. In particular, the strongly scale and position dependent energy injection/release processes associated with anisotropic production by mean shear and inhomogeneous spatial fluxes lead to a geometrically complex redistribution of energy. A split cascade takes place in the space of scales analogously to that in physical space. In other words, energy produced in the near-wall region splits in physical space to feed both the bulk and wall regions through ascending and descending spatial fluxes and in scale space to feed both larger and smaller scales through reverse and forward cascades [5, 6, 7]. The singularity point for the split in physical space is $z^+ \approx 16$ while for the split in the space of scales is $r_y^+ \approx 70$ (here z is the wall distance while r_y is the spanwise scale and $+$ denotes non-dimensionalization in friction units). These values can be reasonably considered as Reynolds independent thus showing that the split cascade is not limited to the large-scale motions. In other words, also small-scale theories of turbulence must address the split cascade and the strongly anisotropic and inhomogeneous energy injection processes causing it. A major issue for the development of such a small-scale theory is represented by the reverse energy cascade phenomenon. This is particularly evident for turbulence closures such as those for large-eddy simulation [8, 9, 10, 11, 12, 13]. Energy should emerge from nowhere in the space of small unresolved scales to drive the quasi-coherent dynamics of the large resolved motion.

Several fundamental features of the energy cascade in wall turbulence have been unveiled by using the theoretical framework provided by the so-called generalized Kolmogorov equation, see e.g. [14, 15, 5, 16, 6, 17, 18, 19, 20, 21, 7]. The generalized Kolmogorov equation is an exact evolution equation for the second-order moment of the two-point velocity increment [22]. As a consequence, scale energy is identified as central quantity. However, it is not the only possibility. In fact, a picture based on vorticity is at least an equally interesting perspective. Vorticity is generated at the wall, due to the no-slip condition that allows the wall to generate tangential stresses, and is immediately injected in the fluid domain through diffusion. This injection of vorticity into the domain is in the opposite direction to the momentum flux [23]. In particular, [24] introduced the idea that vorticity is generated at the wall through tangential pressure gradients (and eventual accelerations of the wall), causing a wall-normal vorticity flux in the fluid domain. Subsequently, this concept has been extended to curved walls by [25]. Furthermore, vorticity dynamics also plays a role in the energy cascade process. Indeed, by applying the filtering formalism [26], it is possible to express the kinetic energy cascade rate in terms of the subgrid stresses and of the velocity field gradient, which in turn can be decomposed into a symmetrical (pure strain) and an anti-symmetrical (pure rotation) component [27, 28]. These features make vorticity statistics interesting as they can both give an insight into the topology of the structures involved in wall turbulence and a different view into areas where the energy cascade process is profoundly modified as in the near-wall region with the split cascade phenomenon.

The aim of the present work is to address the split energy cascade in near-wall turbulence through an analysis of the scale-dependent features of vorticity. In particular, an exact equation for the second-order moment of the two-points vorticity increments (hereafter called scale enstrophy) is derived and studied in the settings of a temporal evolving boundary layer.

2 Temporal evolving boundary layer

When dealing with boundary layers, wall turbulence is characterized also by entrainment phenomena at the turbulent/non-turbulent interface [1] whose physical features cannot be addressed in channel and pipe flows. Such phenomena make the study of boundary layers of a more general relevance for industrial and geophysical problems. However, the spatial inhomogeneity in the streamwise direction renders boundary layers more challenging for their study in comparison with streamwise-homogeneous channels and pipes especially when dealing with sophisticated statistical tools based on two-point statistical observables. It should be noted that also the Fourier transform is not applicable in the streamwise direction due to the inhomogeneity in such direction, thus strongly limiting also the use of the formalism given by the spectral energy budget [29, 30, 31]. A method to circumvent all these issues is to consider a temporally evolving boundary layer [32, 33], which has been shown to present statistical features very similar to those of the spatially evolving boundary layer.

The temporal boundary layer consists of an initially stationary fluid with a solid wall at the bottom moving at a constant speed U_w and a free-slip impermeable boundary condition at the top. Periodic boundary conditions are imposed in the x-streamwise and y-spanwise directions. Differently from the more classical spatially developing boundary layer, this flow evolves in time thereby increasing its thickness and friction Reynolds number. The direct numerical simulation considered in the present work reaches a friction Reynolds number $Re_\tau = 1500$. These data have been already employed in [34, 7] to which the reader is referred for further details on the flow and numerical settings. For the sake of completeness,

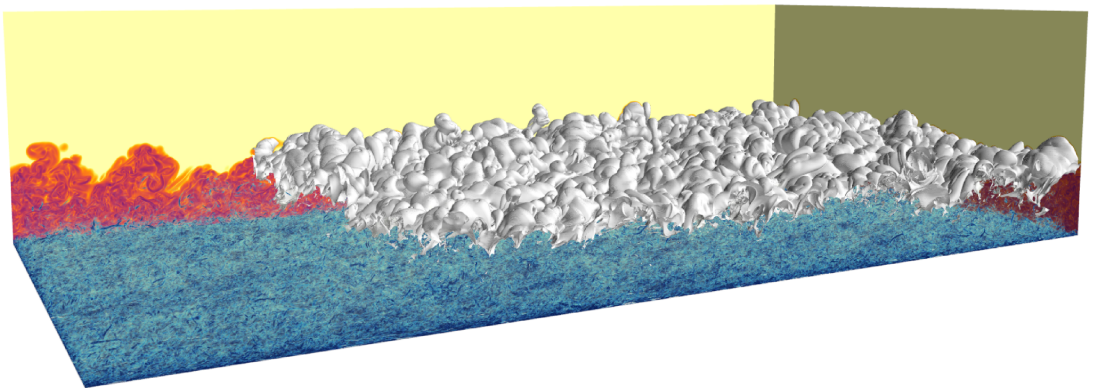

Figure 1: Instantaneous snapshot of the enstrophy field $\zeta = \omega_i\omega_i$ of the temporal boundary layer at $Re_\tau = 1500$. Iso-contours of enstrophy in the slices are reported in logarithmic scale (values increasing from yellow to purple). The grey iso-surface reports $\zeta = 1.4 \cdot 10^{-6}\langle\zeta\rangle_w$ while the iso-surfaces from transparent yellow to opaque blue report increasing values of enstrophy.

here we report only the features. The simulations have been carried out using the solver CaNS [35] that employs a standard pressure-projection method and a staggered second-order finite-difference scheme for the spatial discretization. Time integration is carried out using a mixed approach, Crank–Nicholson for the integration of the viscous terms in the wall-normal direction are integrated implicitly through the use of a Crank–Nicholson scheme, while a three-step Runge–Kutta method with a condition $CFL = 0.95$ for all the other terms. The domain dimension evaluated at the end of the simulation where the boundary layer thickness δ is maximum is $(L_x, L_y, L_z) = (11.9\delta, 5.9\delta, 2, 8\delta)$. The number of grid points employed is $(N_x, N_y, N_z) = (3072, 3072, 768)$ that leads to a spatial resolution evaluated in friction units at the end of the simulation $(\Delta x^+, \Delta x^+, \Delta z_w^+) = (5.8, 2.9, 0.09)$. An instantaneous snapshot showing the topology of the flow is reported in figure 1.

In what follows, the standard Reynolds decomposition is adopted and denoted as $u_i^* = U_i + u_i$, where u_i^* is the total velocity field, while $U_i = \langle u_i^* \rangle$ and u_i are respectively the mean and fluctuating velocity fields. The average operator $\langle\cdot\rangle$ is hereafter computed by spatial averaging in the wall-parallel homogeneous directions (x and y) and by ensemble averaging between four independent realizations of the flow.

3 Two-point enstrophy budget

Turbulent enstrophy is defined as $\zeta = \omega_i\omega_i$ where ω_i is the fluctuating vorticity vector. Enstrophy is an observable closely related to the very nature of turbulence, given its close connection with dissipation and with its rotational nature. While the latter is obvious by its very definition, the former is demonstrated by the fact that

$$\epsilon = \nu\zeta + \nu\frac{\partial^2 u_i u_j}{\partial x_i \partial x_j}, \tag{1}$$

where $\epsilon = \nu(\partial u_i/\partial x_j)(\partial u_i/\partial x_j)$ is the pseudo-dissipation. The fact that enstrophy represents a fundamental mechanisms at the basis of dissipation is even more evident in statistically homogeneous isotropic conditions where $\langle\epsilon\rangle = \nu\zeta$.

A way to address the scale-dependence of enstrophy is to consider its second-order structure function,

$$\langle\delta\zeta^2\rangle \equiv \langle\delta\omega_i\delta\omega_i\rangle \tag{2}$$

where $\delta\omega_i = \omega_i(\boldsymbol{x}'', t) - \omega_i(\boldsymbol{x}', t)$ is the fluctuating vorticity increment. In analogy with [22], the second-order moment of vorticity increment (2) will be herefater called scale enstrophy. The statistical features of the scale enstrophy are better expressed by considering the two-point separation vector $\boldsymbol{r} = \boldsymbol{x}'' - \boldsymbol{x}'$ and the midpoint vector $\boldsymbol{x_c} = (\boldsymbol{x}'' + \boldsymbol{x}')/2$, i.e. $\delta\zeta^2 = \delta\zeta^2(\boldsymbol{x_c}, \boldsymbol{r}, t)$. The dependence of scale enstrophy on the midpoint $\boldsymbol{x_c}$ is related to the statistical inhomogeneity of the flow while the dependence on the separation vector $\boldsymbol{r}$ is related to the multiscale features of the flow.

The exact evolution equation for scale (2) can be directly derived from the vorticity equations following a procedure that has been introduced by [22] for the second-order structure function of velocity, see also

[36]. In its more general form, the equation reads

$$\begin{aligned}
&\frac{\partial\langle\delta\zeta^2\rangle}{\partial t}+\underbrace{\frac{\partial\langle\delta\zeta^2\widetilde{u}_j\rangle}{\partial x_{c_j}}+\frac{\partial\langle\delta\zeta^2\rangle\widetilde{U}_j}{\partial x_{c_j}}-\frac{\nu}{2}\frac{\partial^2\langle\delta\zeta^2\rangle}{\partial x_{c_j}\partial x_{c_j}}}_{\text{spatial transport}}+\underbrace{\frac{\partial\langle\delta\zeta^2\delta u_j\rangle}{\partial r_j}+\frac{\partial\langle\delta\zeta^2\rangle\delta U_j}{\partial r_j}-2\nu\frac{\partial^2\langle\delta\zeta^2\rangle}{\partial r_j\partial r_j}}_{\text{scale transport}}=\\
&\qquad\underbrace{2\langle\delta\omega_i\delta\omega_j\widetilde{\left(\frac{\partial u_i}{\partial x_j}\right)}\rangle+2\langle\delta\omega_i\widetilde{\omega}_j\,\delta\left(\frac{\partial u_i}{\partial x_j}\right)\rangle}_{\text{vortex stretching}}\\
&\underbrace{+2\langle\delta\omega_i\delta\omega_j\rangle\widetilde{\left(\frac{\partial U_i}{\partial x_j}\right)}+2\langle\delta\omega_i\widetilde{\omega}_j\rangle\,\delta\left(\frac{\partial U_i}{\partial x_j}\right)+2\delta\Omega_j\langle\delta\omega_i\widetilde{\left(\frac{\partial u_i}{\partial x_j}\right)}\rangle+2\widetilde{\Omega}_j\langle\delta\omega_i\,\delta\left(\frac{\partial u_i}{\partial x_j}\right)\rangle}_{\text{vortex stretching}}\\
&\qquad\underbrace{-2\langle\delta\omega_i\delta u_j\rangle\widetilde{\left(\frac{\partial\Omega_i}{\partial x_j}\right)}-2\langle\delta\omega_i\widetilde{u}_j\rangle\,\delta\left(\frac{\partial\Omega_i}{\partial x_j}\right)-4\langle\widetilde{\epsilon_\zeta}\rangle}_{\text{source}}
\end{aligned}\tag{3}$$

where $\Omega_i=\langle\omega_i\rangle$ is the average vorticity vector,

$$\epsilon_\zeta=\nu\frac{\partial\omega_i}{\partial x_j}\frac{\partial\omega_i}{\partial x_j}\tag{4}$$

is the dissipation of enstrophy and the operator $\widetilde{\cdot}$ denotes the two-point average. Equation (3) represents an exact equation that statistically describes all the degrees of freedom of turbulence by addressing the augmented space of scales and positions, $\boldsymbol{r}$ and $\boldsymbol{x_c}$ respectively. Hence, the multiscale nature of turbulence also in strongly inhomogeneous and anisotropic conditions is formally described by this theoretical framework. In order to highlight the physical processes described, the two-point enstrophy equation can be recasted in a conservative form as

$$\frac{\partial\langle\delta\zeta^2\rangle}{\partial t}+\nabla_6\cdot\boldsymbol{\phi}=\xi\tag{5}$$

Hence, the two-point enstrophy equation describe a balance between a hyperflux occurring both in physical and scale space

$$\boldsymbol{\phi}=\begin{bmatrix}\boldsymbol{\phi_c}\\ \boldsymbol{\phi_r}\end{bmatrix}=\begin{bmatrix}
\langle\delta\zeta^2\widetilde{u}\rangle+\langle\delta\zeta^2\rangle\widetilde{U}-\frac{\nu}{2}\frac{\partial\langle\delta\zeta^2\rangle}{\partial x_c}\\
\langle\delta\zeta^2\widetilde{v}\rangle+\langle\delta\zeta^2\rangle\widetilde{V}-\frac{\nu}{2}\frac{\partial\langle\delta\zeta^2\rangle}{\partial y_c}\\
\langle\delta\zeta^2\widetilde{w}\rangle+\langle\delta\zeta^2\rangle\widetilde{W}-\frac{\nu}{2}\frac{\partial\langle\delta\zeta^2\rangle}{\partial z_c}\\
\langle\delta\zeta^2\delta u\rangle+\langle\delta\zeta^2\rangle\delta U-2\nu\frac{\partial\langle\delta\zeta^2\rangle}{\partial r_x}\\
\langle\delta\zeta^2\delta v\rangle+\langle\delta\zeta^2\rangle\delta V-2\nu\frac{\partial\langle\delta\zeta^2\rangle}{\partial r_y}\\
\langle\delta\zeta^2\delta w\rangle+\langle\delta\zeta^2\rangle\delta W-2\nu\frac{\partial\langle\delta\zeta^2\rangle}{\partial r_z}
\end{bmatrix}\tag{6}$$

and a net source/sink term

$$\xi=\chi+\mathcal{S}-4\langle\widetilde{\epsilon_\zeta}\rangle\tag{7}$$

given by the balance between enstrophy injection by vortex stretching

$$\begin{aligned}
\chi=\;&2\langle\delta\omega_i\delta\omega_j\widetilde{\left(\frac{\partial u_i}{\partial x_j}\right)}\rangle+2\langle\delta\omega_i\widetilde{\omega}_j\,\delta\left(\frac{\partial u_i}{\partial x_j}\right)\rangle+\\
&2\langle\delta\omega_i\delta\omega_j\rangle\widetilde{\left(\frac{\partial U_i}{\partial x_j}\right)}+2\langle\delta\omega_i\widetilde{\omega}_j\rangle\,\delta\left(\frac{\partial U_i}{\partial x_j}\right)+2\delta\Omega_j\langle\delta\omega_i\widetilde{\left(\frac{\partial u_i}{\partial x_j}\right)}\rangle+2\widetilde{\Omega}_j\langle\delta\omega_i\,\delta\left(\frac{\partial u_i}{\partial x_j}\right)\rangle
\end{aligned}\tag{8}$$

by mean vorticity gradient

$$\mathcal{S} = -2\langle\delta\omega_i\delta u_j\rangle\widetilde{\left(\frac{\partial\Omega_i}{\partial x_j}\right)} - 2\langle\delta\omega_i\widetilde{u}_j\rangle\,\delta\left(\frac{\partial\Omega_i}{\partial x_j}\right) \tag{9}$$

and by viscous dissipation of enstrophy $-4\langle\widetilde{\epsilon_\zeta}\rangle$.

The multi-dimensional form of the budget (3), or equivalently (5), challenges for a clear understanding. That is why it is useful to address paradigmatic flows that exhibit statistical symmetries that can be exploited to reduce the dimensionality of the problem. This is exactly the great advantage provided by the temporal boundary layer compared with the spatially evolving boundary layer. In fact, the statistical homogeneity in both the streawise and spanwise directions drastically reduces the dimensionality of the problem from 6 to 4 dimensions, the three-dimensional space of scales and the wall distance. Hence, the reduced form of the two-point enstrophy budget for the symmetries of the temporal boundary layer reads

$$\begin{aligned}
&\frac{\partial\langle\delta\zeta^2\rangle}{\partial t} + \underbrace{\frac{\partial\langle\delta\zeta^2\widetilde{u}_j\rangle}{\partial z_c} - \frac{\nu}{2}\frac{\partial^2\langle\delta\zeta^2\rangle}{\partial z_c\partial z_c}}_{\text{spatial transport}} + \underbrace{\frac{\partial\langle\delta\zeta^2\delta u_j\rangle}{\partial r_j} + \frac{\partial\langle\delta\zeta^2\rangle\delta U}{\partial r_x} - 2\nu\frac{\partial^2\langle\delta\zeta^2\rangle}{\partial r_j\partial r_j}}_{\text{scale transport}} = \\
&\qquad\qquad \underbrace{2\langle\delta\omega_i\delta\omega_j\widetilde{\left(\frac{\partial u_i}{\partial x_j}\right)}\rangle + 2\langle\delta\omega_i\widetilde{\omega}_j\,\delta\left(\frac{\partial u_i}{\partial x_j}\right)\rangle}_{\text{vortex stretching}} \\
&\underbrace{+2\langle\delta\omega_i\delta\omega_j\widetilde{\left(\frac{\partial U}{\partial z}\right)} + 2\langle\delta\omega_i\widetilde{\omega}_j\rangle\,\delta\left(\frac{\partial U}{\partial z}\right) + 2\delta\Omega_y\langle\delta\omega_i\widetilde{\left(\frac{\partial u_i}{\partial x_j}\right)}\rangle + 2\widetilde{\Omega}_y\langle\delta\omega_i\,\delta\left(\frac{\partial u_i}{\partial x_j}\right)\rangle}_{\text{vortex stretching}} \\
&\qquad\qquad \underbrace{-2\langle\delta\omega_i\delta u_j\rangle\widetilde{\left(\frac{\partial\Omega_y}{\partial z}\right)} - 2\langle\delta\omega_i\widetilde{u}_j\rangle\,\delta\left(\frac{\partial\Omega_y}{\partial z}\right) - 4\langle\widetilde{\epsilon_\zeta}\rangle}_{\text{source}}
\end{aligned} \tag{10}$$

thus showing that the spatial flux survives only among different wall distances z_c, contrary to spatially evolving boundary layers where a spatial flux, although weak, survives also in the streamwise direction x_c. To further simplify the theoretical framework, it is possible to limit the analysis to the sole space of horizontal scales, the $(r_z = 0)$-hyperplane as it is commonly done in works employing a spectral decomposition of the flow. In this case the equation reads

$$\begin{aligned}
&\frac{\partial\langle\delta\zeta^2\rangle}{\partial t} + \underbrace{\frac{\partial\langle\delta\zeta^2\widetilde{u}_j\rangle}{\partial z_c} - \frac{\nu}{2}\frac{\partial^2\langle\delta\zeta^2\rangle}{\partial z_c\partial z_c}}_{\text{spatial transport}} + \underbrace{\frac{\partial\langle\delta\zeta^2\delta u_j\rangle}{\partial r_j} - 2\nu\frac{\partial^2\langle\delta\zeta^2\rangle}{\partial r_j\partial r_j}}_{\text{scale transport}} = \\
&\underbrace{2\langle\delta\omega_i\delta\omega_j\widetilde{\left(\frac{\partial u_i}{\partial x_j}\right)}\rangle + 2\langle\delta\omega_i\widetilde{\omega}_j\,\delta\left(\frac{\partial u_i}{\partial x_j}\right)\rangle + 2\langle\delta\omega_i\delta\omega_j\rangle\widetilde{\left(\frac{\partial U}{\partial z}\right)} + 2\widetilde{\Omega}_y\langle\delta\omega_i\,\delta\left(\frac{\partial u_i}{\partial x_j}\right)\rangle}_{\text{vortex stretching}} \\
&\qquad\qquad \underbrace{-2\langle\delta\omega_i\delta u_j\rangle\widetilde{\left(\frac{\partial\Omega_y}{\partial z}\right)} - 4\langle\widetilde{\epsilon_\zeta}\rangle}_{\text{source}}
\end{aligned} \tag{11}$$

and allows us to study how scale enstrophy is generated, transported and finally dissipated among horizontal scales and wall distances. The preliminary results on a temporal boundary layer reported in the next section are based on this last equation.

4 Preliminary results

Vorticity, can only be generated by shear forces, which, in the presented flow settings, can only be introduced by the wall. In particular, the solid wall can only introduce streamwise $\langle\omega_x\omega_x\rangle$ and spanwise $\langle\omega_y\omega_y\rangle$ enstrophy contributions. Enstrophy is then transported away from the wall, initially by pure diffusion (since $w \sim z^2$) and then also via convective turbulent transport. Finally, vortex stretching,

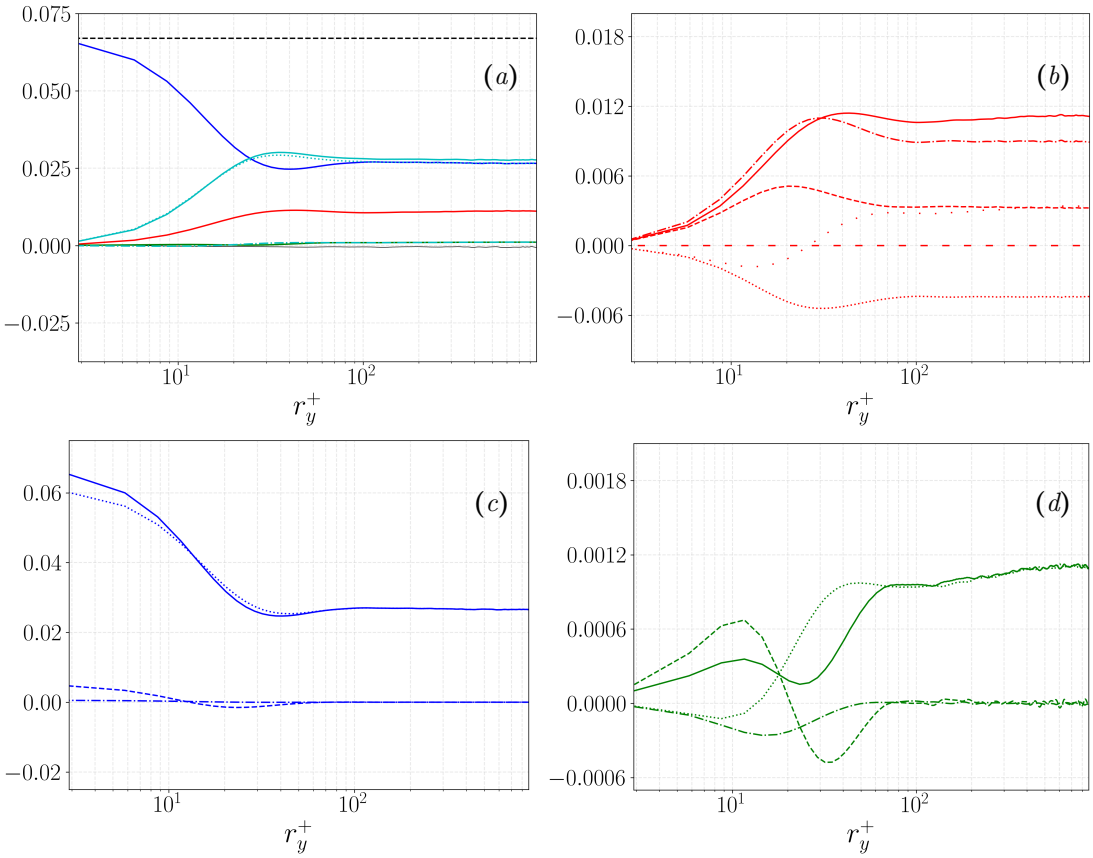

Figure 2: Scale-by-scale budget of turbulent enstrophy in the spanwise scales r_y^+ evaluated at $z_c^+ = 0.5$ and scaled in friction units. The complete budget is reported in (a). The terms of the scale enstrophy equation are reported with different colours: inertial scale transport $-\partial\langle\delta\zeta^2\delta u_j\rangle/\partial r_j$ (green), viscous scale transport $2\nu\partial^2\langle\delta\zeta^2\rangle/\partial {r_j}^2$ (blue), inertial spatial transport $-\partial\langle\delta\zeta^2\widetilde{u}_j\rangle/\partial z_c$ (cyan dash-dotted line), viscous spatial transport $(\nu/2)\partial^2\langle\delta\zeta^2\rangle/\partial z_c^2$ (cyan dotted line), $\chi+\mathcal{S}$ (red), $4\langle\widetilde{\epsilon_\zeta}\rangle$ (dashed black line) and $\partial\langle\delta\zeta^2\rangle/\partial t$ computed as residue (thin solid black line). The source terms are reported in (b): total $\chi+\mathcal{S}$ (solid line), $2\Omega_y\langle\delta\omega_i\delta\left(\partial u_i/\partial y\right)\rangle$ (dash-dotted line), $2\langle\delta\omega_x\delta\omega_z\rangle\partial U/\partial z$ (dotted line), $2\langle\delta\omega_i\widetilde{\omega}_j\delta\left(\partial u_i/\partial x_j\right)\rangle$ (dashed line), $2\langle\delta\omega_i\delta\omega_j\widetilde{(\partial u_i/\partial x_j)}\rangle$ (loosely dotted line) and $\mathcal{S}$ (loosely dashed line). Diffusive transport among scales is reported in (c): total $2\nu\partial^2\langle\delta\zeta^2\rangle/\partial {r_j}^2$ (solid line), $2\nu\partial^2\langle\delta\zeta^2\rangle/\partial r_x^2$ (dash-dotted line), $2\nu\partial^2\langle\delta\zeta^2\rangle/\partial r_y^2$ (dashed line) and $2\nu\partial^2\langle\delta\zeta^2\rangle/\partial r_z^2$ (dotted line). Inertial transport among scales is reported in (d): total $-\partial\langle\delta\zeta^2\delta u_j\rangle/\partial r_j$ (solid line), $-\partial\langle\delta\zeta^2\delta u\rangle/\partial r_x$ (dash-dotted line), $-\partial\langle\delta\zeta^2\delta v\rangle/\partial r_y$ (dashed line) and $-\partial\langle\delta\zeta^2\delta w\rangle/\partial r_z$ (dotted line).

which in addition to pure stretching is also responsible for vortex tilting, accomplish the amplification and redistribution of the vorticity between its various components. The various mechanisms have a well-defined scale distribution that we preliminary analyse here by means of the two-point enstrophy equation. In order to simplify the analysis in this first attempt, we limit our field of investigation to the behaviour in the space of spanwise scales ($r_z = r_x = 0$) of the very-near-wall region.

4.1 Viscous sublayer

In figure 2(a), the enstrophy budget in the spanwise scales r_y at a wall distance $z_c^+ = 0.5$ is reported. As expected at such a wall distance, the dominant mechanisms are the viscous ones. In fact, the main contributions to the budget in this location are the diffusive transports both among scales and in the physical space. However, the vortex stretching term is already active with a non-negligible intensity. From figure 2(b), where the vortex stretching term is decomposed in its four contributions, it appears that its main contribution comes from the term $2\Omega_y\langle\delta\omega_i\delta\left(\partial u_i/\partial y\right)\rangle$, which can be interpreted as the stretching

and tilting of the mean vorticity Ω_y. In particular, this term exhibits a peak at scales compatible with the quasi-streamwise vorticies living in the buffer layer, suggesting that this effect could be caused by the stretching of Ω_y due to the spanwise velocities with alternating sign induced near the wall by the counter rotating quasi-streamwise vortices, corresponding to the $2\Omega_y\langle\delta\omega_y\delta\left(\partial v/\partial y\right)\rangle$ term. On the contrary, the term $2\langle\delta\omega_x\delta\omega_z\rangle\partial U/\partial z$, appears to be negative with a similar shape but with a lower intensity. This anti-correlation may be explained by comparing it term-by-term with the first contribution. In fact, near the wall we may expect $2\Omega_y\langle\delta\omega_x\delta\left(\partial u/\partial y\right)\rangle$ to be the only other relevant component of $2\Omega_y\langle\delta\omega_i\delta\left(\partial u_i/\partial y\right)\rangle$. If this is true, it can be deduced that $2\Omega_y\langle\delta\omega_x\delta\left(\partial u/\partial y\right)\rangle \approx -2\langle\delta\omega_x\delta\omega_z\rangle\partial U/\partial z$, since $\Omega_y = \partial U/\partial z$, and $\delta\omega_z = \delta\left(\partial v/\partial x - \partial u/\partial y\right) \approx -\partial u/\partial y$ near the wall. In correspondence with the mild peak observed in the vortex stretching at $r_y^+ \approx 40$, it is possible to observe a valley in the diffusive scale transport which takes charge of draining the scale enstrophy injected by transporting it towards smaller scales. As shown in figure 2(c), this transport is mainly constituted by the transport across wall-normal scales r_z, reaffirming that, at such wall distances, enstrophy is transported toward smaller r_z scales, corresponding to sharp wall-normal gradients. Thus, in the very-near wall region, the budget may be approximated as

$$-2\nu\frac{\partial^2\langle\delta\zeta^2\rangle}{\partial r_z^2} - \frac{\nu}{2}\frac{\partial^2\langle\delta\zeta^2\rangle}{\partial z_c^2} = 2\Omega_y\langle\delta\omega_i\delta\left(\frac{\partial u_i}{\partial y}\right)\rangle - 4\langle\epsilon_\zeta\rangle. \tag{12}$$

Finally, we report the inertial transport of enstrophy in figure 2(d), which, despite being negligible in intensity, shows some interesting features. In particular, the spanwise transport $\partial\langle\delta\zeta^2\delta v\rangle/\partial r_y$ shows a typical pattern of a direct enstrophy cascade, draining enstrophy from the injection scale and introducing it at smaller scales. On the other hand, the wall-normal inertial transport $\partial\langle\delta\zeta^2\delta w\rangle/\partial r_z$ appears to inject enstrophy at all r_y scales, indicating that also the inertial transport in the wall-normal scales is performing a direct enstrophy transfer.

4.2 Buffer layer

In the buffer layer, the overall budget (reported in figure 3(a) at a wall distance of $z_c^+ = 11$) quickly recovers characteristics typical of homogeneous isotropic turbulence with some obvious differences. Among others, we can observe that in this region the budget results in an overall net source of scale enstrophy. We can also observe a peak in the vortex stretching at $r_y^+ \approx 40$, with the resulting negative valley in the inertial transport draining scale enstrophy from the injection scale. By examining the composition of the various terms, the differences with respect to homogeneous isotropic turbulence are more evident. The vortex stretching term, depicted in figure 3(b), is dominated by the $2\langle\delta\omega_x\delta\omega_z\rangle\partial U/\partial z$ term. This term may be interpreted as the vortex tilting given by the mean velocity gradient, that appears to be the most relevant contribution acting in the buffer layer. Apparently, the production of enstrophy in the buffer layer is sustained by the combined effect of the mean velocity shear and of vorticity tilted at an angle, hence retaining both a streamwise and a vertical component. The diffusive scale transport, shown in figure 3(c), appears to be still dominated by the transport across wall-normal scales. Finally, in figure 3(d), the inertial transport contributions are shown. As already mentioned, the local minimum in the inertial transport is found to correspond with the enstrophy injection scale $r_y^+ \approx 40$.

As a first approximation, we may express the scale-by-scale budget in the buffer layer as

$$\frac{\partial\langle\delta\zeta^2\rangle}{\partial t} + \frac{\partial\langle\delta\zeta^2\delta u_j\rangle}{\partial r_j} - 2\nu\frac{\partial^2\langle\delta\zeta^2\rangle}{\partial r_z^2} = 2\langle\delta\omega_x\delta\omega_z\rangle\frac{\partial U}{\partial z} + 2\langle\delta\omega_i\widetilde{\omega}_j\delta\left(\frac{\partial u_i}{\partial x_j}\right)\rangle + 2\langle\delta\omega_i\delta\omega_j\widetilde{\left(\frac{\partial u_i}{\partial x_j}\right)}\rangle - 4\langle\epsilon_\zeta\rangle \tag{13}$$

This equation resembles the budget in homogeneous isotropic turbulence with the additional contribution to vortex stretching provided by mean shear, $2\langle\delta\omega_x\delta\omega_z\rangle\partial U/\partial z$ and with the simplification that diffusive scale transport is mainly active in the r_z wall-normal scales.

5 Conclusions

With the aim of understanding the physical mechanisms at the basis of the split energy cascade characterizing wall turbulence in the near-wall region, we introduce a theoretical framework for the study of enstrophy able to describes all the degrees of freedom of turbulence by addressing the augmented space of scales and positions, $\boldsymbol{r}$ and $\boldsymbol{x_c}$ respectively. The multiscale nature of turbulence is formally described by this theoretical framework also in strongly inhomogeneous and anisotropic conditions. A preliminary analysis of the potential of this statistical approach is reported by addressing the scale-by-scale enstrophy budget in the very-near wall region of a temporally evolving boundary layer at a friction Reynolds number $Re_\tau = 1500$. Interesting flow features are shown to be unveiled by the provided formalism thus supporting the advancement of this line of research in future works.

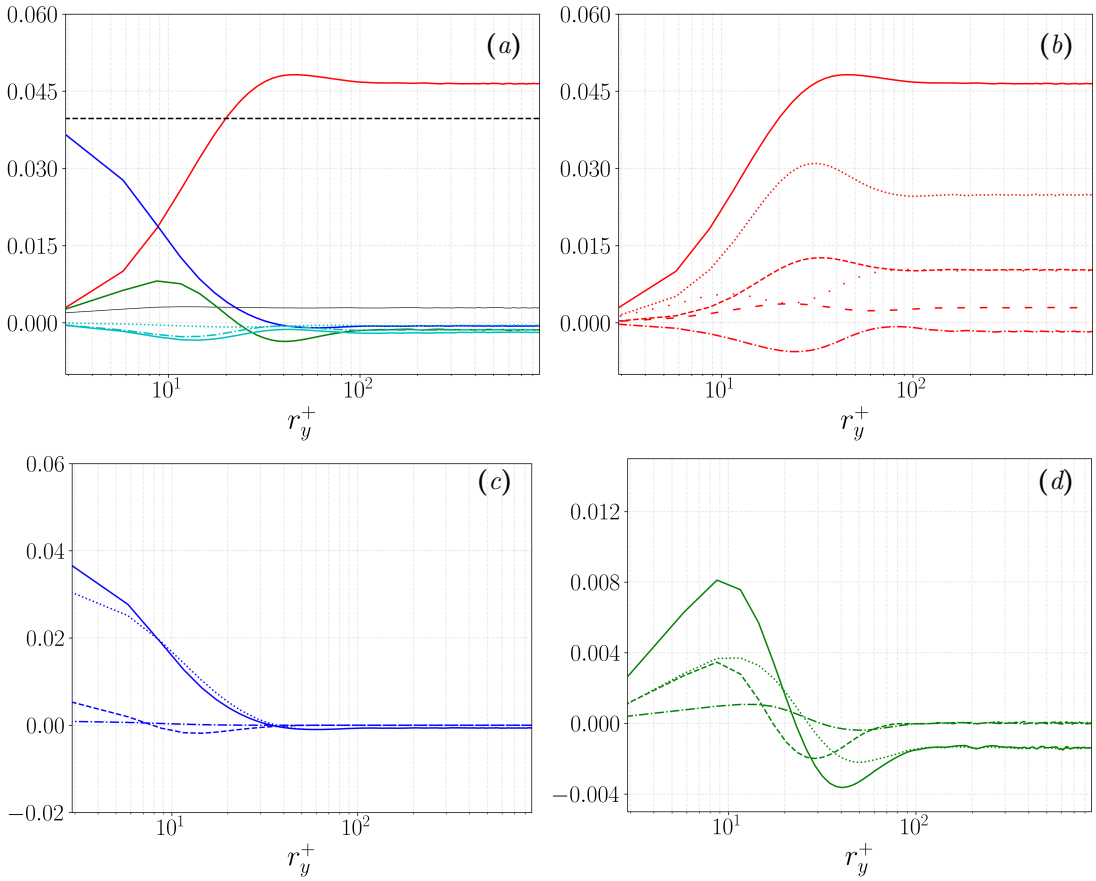

Figure 3: Scale-by-scale budget of turbulent enstrophy in the spanwise scales r_y^+ evaluated at $z_c^+ = 11$ and scaled in friction units. The complete budget is reported in (a). The terms of the scale enstrophy equation are reported with different colours: inertial scale transport $-\partial\langle\delta\zeta^2\delta u_j\rangle/\partial r_j$ (green), viscous scale transport $2\nu\partial^2\langle\delta\zeta^2\rangle/\partial {r_j}^2$ (blue), inertial spatial transport $-\partial\langle\delta\zeta^2\widetilde{u}_j\rangle/\partial z_c$ (cyan dash-dotted line), viscous spatial transport $(\nu/2)\partial^2\langle\delta\zeta^2\rangle/\partial z_c^2$ (cyan dotted line), $\chi+\mathcal{S}$ (red), $4\langle\widetilde{\epsilon_\zeta}\rangle$ (dashed black line) and $\partial\langle\delta\zeta^2\rangle/\partial t$ computed as residue (thin solid black line). The source terms are reported in (b): total $\chi+\mathcal{S}$ (solid line), $2\Omega_y\langle\delta\omega_i\delta\,(\partial u_i/\partial y)\rangle$ (dash-dotted line), $2\langle\delta\omega_x\delta\omega_z\rangle\partial U/\partial z$ (dotted line), $2\langle\delta\omega_i\widetilde{\omega}_j\delta\,(\partial u_i/\partial x_j)\rangle$ (dashed line), $2\langle\delta\omega_i\delta\omega_j(\widetilde{\partial u_i/\partial x_j})\rangle$ (loosely dotted line) and $\mathcal{S}$ (loosely dashed line). Diffusive transport among scales is reported in (c): total $2\nu\partial^2\langle\delta\zeta^2\rangle/\partial {r_j}^2$ (solid line), $2\nu\partial^2\langle\delta\zeta^2\rangle/\partial r_x^2$ (dash-dotted line), $2\nu\partial^2\langle\delta\zeta^2\rangle/\partial r_y^2$ (dashed line) and $2\nu\partial^2\langle\delta\zeta^2\rangle/\partial r_z^2$ (dotted line). Inertial transport among scales is reported in (d): total $-\partial\langle\delta\zeta^2\delta u_j\rangle/\partial r_j$ (solid line), $-\partial\langle\delta\zeta^2\delta u\rangle/\partial r_x$ (dash-dotted line), $-\partial\langle\delta\zeta^2\delta v\rangle/\partial r_y$ (dashed line) and $-\partial\langle\delta\zeta^2\delta w\rangle/\partial r_z$ (dotted line).

References

[1] C. B. da Silva, J. C. R. Hunt, I. Eames, and J. Westerweel. Interfacial layers between regions of different turbulence intensity. *Annu. Rev. Fluid Mech.*, 46:567–590, 2014.

[2] A.A. Townsend. *The structure of turbulent shear flows.* Cambridge University Press, 1976.

[3] S.K. Robinson. Coherent motions in the turbulent boundary layer. *Annu. Rev. Fluid Mech.*, 23:601–639, 1991.

[4] J. Jimenez and A. Pinelli. The autonomous cycle of near-wall turbulence. *J. Fluid Mech.*, 389:335–359, 1999.

[5] A. Cimarelli, E. De Angelis, and C.M. Casciola. Paths of energy in turbulent channel flows. *J. Fluid Mech.*, 715:436–451, 2013.

[6] A. Cimarelli, E. De Angelis, J. Jiménez, and C.M. Casciola. Cascades and wall-normal fluxes in turbulent channel flows. *J. Fluid Mech.*, 796:417–436, 2016.

[7] A. Cimarelli, G. Boga, A. Pavan, P. Costa, and E. Stalio. Spatially evolving cascades in wall turbulence with and without interface. *J. Fluid Mech.*, 987:A4, 2024.

[8] U. Piomelli, W. H. Cabot, P. Moin, and S. Lee. Subgrid-scale backscatter in turbulent and transitional flows. *Phys. Fluids A*, 3(7):1766–1771, 1991.

[9] J. A. Domaradzki, W. Liu, C. Härtel, and L. Kleiser. Energy transfer in numerically simulated wall-bounded turbulent flows. *Phys. Fluids*, 6(4):1583–1599, 1994.

[10] C. Härtel, L. Kleiser, F. Unger, and R. Friedrich. Subgrid-scale energy transfer in the near-wall region of turbulent flows. *Phys. Fluids*, 6(9):3130–3143, 1994.

[11] D. C. Dunn and J. F. Morrison. Analysis of the energy budget in turbulent channel flow using orthogonal wavelets. *Computers & Fluids*, 34(2):199–224, 2005.

[12] A. Cimarelli and E. De Angelis. Anisotropic dynamics and sub-grid energy transfer in wall-turbulence. *Phys. Fluids*, 24(1):015102, 2012.

[13] A. Cimarelli and E. De Angelis. The physics of energy transfer toward improved subgrid-scale models. *Phys. Fluids*, 26(5):055103, 2014.

[14] L. Danaila, F. Anselmet, T. Zhou, and R. A. Antonia. Turbulent energy scale budget equations in a fully developed channel flow. *J. Fluid Mech.*, 430:87–109, 2001.

[15] N. Marati, C.M. Casciola, and R. Piva. Energy cascade and spatial fluxes in wall turbulence. *J. Fluid Mech.*, 521:191–215, 2004.

[16] A. Cimarelli, E. De Angelis, P. Schlatter, G. Brethouwer, A. Talamelli, and C. M. Casciola. Sources and fluxes of scale energy in the overlap layer of wall turbulence. *J. Fluid Mech.*, 771:407–423, 2015.

[17] F. Hamba. Turbulent energy density in scale space for inhomogeneous turbulence. *J. Fluid Mech.*, 842:532–553, 2018.

[18] F. Hamba. Inverse energy cascade and vortical structure in the near-wall region of turbulent channel flow. *Phys. Rev. Fluids*, 4(11):114609, 2019.

[19] D. Gatti, A. Chiarini, A. Cimarelli, and M. Quadrio. Structure function tensor equations in inhomogeneous turbulence. *J. Fluid Mech.*, 898:A5, 2020.

[20] S. J. Zimmerman, R. A. Antonia, L. Djenidi, J. Philip, and J. C. Klewicki. Approach to the 4/3 law for turbulent pipe and channel flows examined through a reformulated scale-by-scale energy budget. *J. Fluid Mech.*, 931:A28, 2022.

[21] A. Apostolidis, J.-P. Laval, and J. C. Vassilicos. Turbulent cascade in fully developed turbulent channel flow. *J. Fluid Mech.*, 967:A22, 2023.

[22] R.J. Hill. Exact second-order structure-function relationship. *J. Fluid Mech.*, 468:317–326, 2002.

[23] G. L. Eyink. Turbulent flow in pipes and channels as cross-stream "inverse cascades" of vorticity. *Phys. Fluids*, 20(12), 2008.

[24] M. J. Lighthill. Introduction boundary layer theory. *Laminar boundary layers*, 1963.

[25] F. A. Lyman. Vorticity production at a solid boundary. *Appl. Mech. Rev*, 43(8):157–158, 1990.

[26] M. Germano. Turbulence: the filtering approach. *J. Fluid Mech.*, 238:325–336, 1992.

[27] C. Meneveau. Lagrangian dynamics and models of the velocity gradient tensor in turbulent flows. *Annu. Rev. Fluid Mech.*, 43(1):219–245, 2011.

[28] P. L. Johnson and M. Wilczek. Multiscale velocity gradients in turbulence. *Annu. Rev. Fluid Mech.*, 56(1):463–490, 2024.

[29] Y. Mizuno. Spectra of energy transport in turbulent channel flows for moderate reynolds numbers. *J. Fluid Mech.*, 805:171–187, 2016.

[30] M. Cho, Y. Hwang, and H. Choi. Scale interactions and spectral energy transfer in turbulent channel flow. *J. Fluid Mech.*, 854:474–504, 2018.

[31] M. Lee and R. D. Moser. Spectral analysis of the budget equation in turbulent channel flows at high reynolds number. *J. Fluid Mech.*, 860:886–938, 2019.

[32] M. Kozul, D. Chung, and J. P. Monty. Direct numerical simulation of the incompressible temporally developing turbulent boundary layer. *J. Fluid Mech.*, 796:437–472, 2016.

[33] X. Zhang, T. Watanabe, and K. Nagata. Reynolds number dependence of the turbulent/non-turbulent interface in temporally developing turbulent boundary layers. *J. Fluid Mech.*, 964:A8, 2023.

[34] A. Cimarelli, G. Boga, A. Pavan, P. Costa, and E. Stalio. Energy cascade phenomena in temporal boundary layers. *Flow Turb. Comb.*, 112:129–145, 2024.

[35] P. Costa. A FFT-based finite-difference solver for massively-parallel direct numerical simulations of turbulent flows. *Comput. & Math. App.*, 76(8):1853–1862, 2018.

[36] P. Baj, F. A. Portela, and D. W. Carter. On the simultaneous cascades of energy, helicity, and enstrophy in incompressible homogeneous turbulence. *J. Fluid Mech.*, 952:A20, 2022.